


Intense boundary emission destroys normal radio-frequency plasma sheathGuang-Yu Sun , An-Bang Sun , and Guan-Jun Zhang**Research Center for Advanced High Voltage and Plasma Technology, State Key Laboratory of Electrical Insulation and Power Equipment, Xi'an Jiaotong University, Xi'an, Shaanxi 710049, China* (Received 2 September 2019; revised manuscript received 5 January 2020; accepted 12 February 2020; published 4 March 2020)

The plasma sheath is the non-neutral space charge region that isolates bulk plasma from a boundary. Radio-frequency (RF) sheaths are formed when applying RF voltage to electrodes. Generally, applied bias is mainly consumed by a RF sheath, which shields an external field. Here we report evidence that an intense boundary emission destroys a normal RF sheath and establishes a type of RF plasma where external bias is consumed by bulk plasma instead of a sheath. Ions are naturally confined while plasma electrons are unobstructed, generating a strong RF current in the entire plasma, combined with a unique particle and energy balance. The proposed model offers the possibility for ion erosion mitigation of a plasma-facing component. It also inspires techniques for reaction rate control in plasma processing and wave mode conversion.

DOI: [10.1103/PhysRevE.101.033203](https://doi.org/10.1103/PhysRevE.101.033203)**I. INTRODUCTION**

Plasma sheaths are one of the most ubiquitous and well-known features that permeate laboratory plasmas as most confined plasmas have boundaries [1–5]. Dating back to around a century ago when Irving Langmuir first introduced the term “sheath” to describe an ion-rich region adjacent to the electrode [6], studies of sheaths have since been developing rapidly and are still of vital importance in modern plasma physics. Sheaths matter in fusion devices [1,2,7,8], dusty plasma [3,9,10], spacecraft propulsion [11,12], plasma diagnostics, material processing [13,14], and many other areas [5,15,16].

Applying radio-frequency (RF) voltage to electrodes creates a capacitively coupled plasma (CCP) with two oscillating RF sheaths. Understanding RF sheaths is of fundamental interest and is essential in numerous applications [13,14,17–21]. Contemporary CCP models assume that the bulk plasma is well isolated from boundaries by sheaths, and applied bias mainly rests on sheaths instead of bulk plasma. A conduction current dominates over a displacement current in bulk plasma, while the field in bulk plasma is shielded. However, in this work we will show that the bias can be primarily consumed by bulk plasma, and the electric field in plasma center does not need to be shielded by sheaths, due to intense boundary emission.

Many studies have been performed on CCP boundary emission, but its influence is mostly assumed to be unessential [20,22–29]. The steady flux of an ion Γ_i produces a surface emission flux $\Gamma_{em} = \gamma_i \Gamma_i$ due to ion-induced secondary electron emission (SEE), with γ_i the ion-induced secondary electron emission coefficient. Under low pressure, secondary electrons (SEs) are lost before remarkable ionizations occur, and their impact is less significant than that of hot electrons

generated by stochastic heating [30]. Higher pressure incurs a transition to the γ mode where ionizations of SEs become dominant [24]. Yet the structure of plasma, i.e., bulk plasma connected by a Bohm presheath and Child-law sheath, is retained, and the mean wall potential remains negative relative to plasma [31–35].

In this work, we show that intense boundary emission creates remarkable influence and restructures the entire RF plasma, which happens when Γ_{em} is greater than the plasma electron flux Γ_{ep} on average. It is well known that a space-charge-limited (SCL) sheath is formed if $\Gamma_{em} > \Gamma_{ep}$ near the plasma boundary, such as a thermionic emitter, emissive probe, Hall thruster, etc. [36–38]. In this case, a normal Child-law sheath still exists between plasma and the local potential minimum called a virtual cathode (VC), so plasma dynamics are not essentially modified [39]. Recent works reported that a floating SCL sheath cannot remain stable due to cold ion accumulation in a VC [40,41]. But no one to our knowledge has studied a RF plasma with intense boundary emission. Below we shall first show with a simulation how a RF plasma behaves under strong boundary emission; a theoretical ground is then given to validate simulation results. Model generality, practical methods for implementation, and prospects in future applications are discussed as well.

II. MODEL SETUP

To investigate a RF plasma with boundary emission, we employ a 1D1V (one spatial and one velocity domain) continuum kinetic simulation code that advances the kinetic equation and solves the Poisson equation in each step. The use of a continuum kinetic simulation has proved powerful in numerous works related to boundary plasma physics [42–46]. Kinetic simulation produces smooth data free from noise and allows convenient control of plasma density, temperature and velocity distribution function (VDF), etc. In our simulation, a RF plasma bounded by two parallel planar electrodes is

*gjzhang@xjtu.edu.cn

considered. A sinusoidal source is fixed as a Dirichlet-type condition at two boundaries. The initial state is a uniform Maxwellian distribution in space for both electrons and ions: $f_{s0}(x, v) = n_0 \sqrt{\frac{m_s}{2\pi T_s}} \exp(-\frac{m_s v^2}{2T_s})$. Here subscript s represents ion (i) or electron (e), n_0 is initial plasma density, and m , T , v are mass, temperature, and velocity, respectively. After simulation begins, the VDFs are advanced according to the kinetic equation

$$\begin{aligned} \frac{\partial f_s(x, v)}{\partial t} + v \frac{\partial f_s(x, v)}{\partial x} + \frac{q_s [E + v \times B]}{m_s} \frac{\partial f_s(x, v)}{\partial v} \\ = S_{\text{charge}} + S_{\text{collision},s} \end{aligned} \quad (2.1)$$

with q_s being the particle charge, E and B fields at location x , and f_s the distribution function depending on time t , location x , and velocity v . Equation (2.1) includes four advections which dictate the evolution of VDF, namely, $-v \frac{\partial f_s(x, v)}{\partial x}$, $-\frac{q_s [E(x) + v \times B]}{m_s} \frac{\partial f_s(x, v)}{\partial v}$, S_{charge} , and $S_{\text{collision},s}$. They are the space advection, velocity advection, source term, and collision term, respectively. Note that the time step, space, and velocity resolution are controlled to satisfy the Courant-Friedrichs-Lewy stability condition. Also, the velocity advection requires the solution of a one-dimensional (1D) Poisson equation, which is solved with the finite difference method. Detailed definitions of source and collision terms are provided below.

A source term compensates particle loss at boundaries. One approach is to generate electron-ion pairs according to velocity-dependent ionization, i.e., $S_{\text{charge}} = f_{s0} v_e n_g \sigma_{iz}$, with v_e the electron velocity (more precisely relative velocity), n_g background gas density, and σ_{iz} cross section determined by the electron kinetic energy. In our simulation, the plasma density is expected to be controlled as constant to facilitate comparison with theory, so the following expression is adopted:

$$S_{\text{charge}} = \frac{\Gamma_{i,L} + \Gamma_{i,R}}{n_0 L_s} f_{s0} \quad (2.2)$$

with $\Gamma_{i,L/R}$ the ion flux at left/right wall and L_s the length where source is supplied. In this way, the ion lost at boundaries is compensated by Maxwellian electron-ion pairs generated by the source term.

The collision term characterizes the change of distribution function due to particle collision. The collision term for electrons is defined as

$$S_{\text{collision},e} = \frac{v_{\text{TeP}}}{\lambda_e} \left(\frac{n_e}{n_0} f_{e0} - f_e \right), \quad (2.3)$$

where $v_{\text{TeP}} = \sqrt{\frac{T_{\text{ep}}}{m_e}}$, T_{ep} is the temperature of plasma electrons, λ_e is electron mean-free path, and n_e is electron density at position x . With Eq. (2.3), electrons that encounter a collision are replaced by an equal number of electrons following a Maxwellian distribution. λ_e is set to be greater than sheath size and much smaller than the total length of simulation domain, representing a typical collisionless sheath. For ions

the following operator is used:

$$S_{\text{collision},i} = \frac{\int_{-\infty}^{+\infty} v_i f_i d v_i}{n_0} \frac{f_{i0}}{\lambda_i} - \frac{|v_i|}{\lambda_i} f_i, \quad (2.4)$$

where λ_i is ion mean-free path usually greater than sheath size, and v_i is ion velocity. Equation (2.4) represents charge exchange collisions for ions, which removes fast ions from f_i at each position x and replaces them with an equal number of cold ions following f_{i0} . The charge exchange collision frequency is proportional to ion velocity. The validity of the above two collision terms has been justified in previous works [40,47,48].

Surface emission is characterized by the EVDF boundary condition in the following way (taking the left boundary as an example):

$$f_e(x = 0, v_e > 0) = \frac{m_e}{T_{\text{em}}} \Gamma_{\text{em}} \exp\left(-\frac{m_e v_e^2}{2T_{\text{em}}}\right). \quad (2.5)$$

Here Γ_{em} is the surface emission flux and T_{em} is the temperature of emitted electrons. For thermionic emission and photoemission, Γ_{em} is a constant depending on the electrode temperature or light intensity. For ion distribution, the RHS of Eq. (2.5) is zero. For secondary electron emission induced by electrons, it is

$$f_e(x = 0, v_e > 0) = \frac{m_e}{T_{\text{em}}} \gamma_e \Gamma_{\text{ep}} \exp\left(-\frac{m_e v_e^2}{2T_{\text{em}}}\right), \quad (2.6)$$

where $\gamma_e = \frac{\Gamma_{\text{em}}}{\Gamma_{\text{ep}}}$ is the electron-induced secondary electron emission coefficient.

Detailed adopted parameters are given below to help replicate presented data. $n_0 = 5 \times 10^{14} \text{ m}^{-3}$, $T_{\text{ep}} = 14 \text{ eV}$, $T_{\text{em}} = 2.5 \text{ eV}$, $T_i = 0.05 \text{ eV}$, and ion mass $1u$. $\lambda_e = 1.25 \text{ cm}$ and $\lambda_i = 0.3 \text{ cm}$. $L = 10 \text{ cm}$, and space resolution $\Delta x = 10^{-4} \text{ m}$. The range of the electron/ion velocity is $4v_{\text{TeP}}$ and $2c_s$, with $v_{\text{TeP}} = \sqrt{\frac{T_{\text{ep}}}{m_e}}$ and $c_s = \sqrt{\frac{T_{\text{ep}}}{m_i}}$, divided into 601 points. The time step is $\Delta t = 2 \times 10^{-3} \text{ ns}$, and source frequency is 13.56 MHz .

III. RESULTS

For a normal RF sheath, the flux balance on average should be fulfilled, which means that $\langle \Gamma_{\text{ep}} - \Gamma_i - \Gamma_{\text{em}} \rangle_T = 0$. In typical RF discharge, $\omega_i \ll \omega \ll \omega_e$ with ω_i , ω_e the ion and electron frequency, and ω the source frequency. In this case, ions respond to time-averaged space potential, so flux balance is simplified as $\langle \Gamma_{\text{ep}} - \Gamma_{\text{em}} \rangle_T = \Gamma_i = n_{\text{sh}} u_B$ where n_{sh} is the plasma density at the sheath edge and u_B is the Bohm velocity. The Bohm velocity is crucial in plasma sheath theory. Its value is influenced by collisionality, while a recent study of Tang and Guo indicates that electron heat flux also plays a critical role [49].

However, when boundary emission is greater than plasma electron flux, the normal flux balance no longer holds since ion flux should be non-negative, which indicates that classical CCP breaks down when $\langle \Gamma_{\text{ep}} - \Gamma_{\text{em}} \rangle_T < 0$. In order to investigate the RF structure under intense boundary emission, a simulation is performed with $\langle \Gamma_{\text{ep}} - \Gamma_{\text{em}} \rangle_T < 0$, and a constant $\Gamma_{\text{em}} = 10^{21} \text{ m}^{-2} \text{ s}^{-1}$ is used (roughly two times Γ_{ep}). Results are shown Fig. 1(a) where two tiny sheath barriers with positive potential relative to the sheath edge are present near

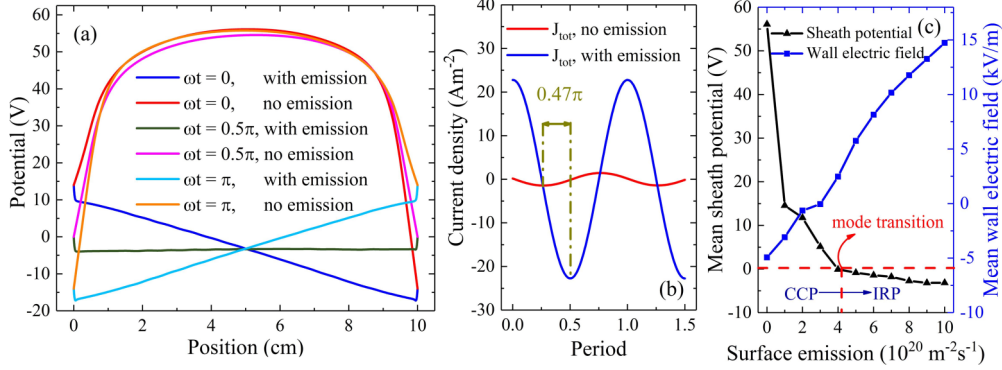


FIG. 1. Simulation results of RF plasma with and without boundary emission. In (a) potentials of normal CCP are compared to a condition with surface emission of $10^{21} \text{ m}^{-2} \text{ s}^{-1}$, which is around twice the initial plasma electron flux. Applied bias is consumed by bulk plasma, and two small sheaths opposite to normal RF sheaths appear at both ends. In (b) the total currents of RF discharge with and without strong boundary emission are compared. They have a phase difference of nearly 0.5π and the boundary emission enlarges the total current by more than one order of magnitude. The external source is $V_{\text{RF}} \cos(\omega t)$. (c) The transition from a normal RF plasma (CCP) to inverted RF plasma when increasing Γ_{em} . Mean sheath potential and mean electric field of the left wall are recorded with different boundary emissions. For convention, mean sheath potential in CCP is chosen as positive, which becomes negative after $\langle \Gamma_{\text{ep}} - \Gamma_{\text{em}} \rangle_T < 0$ (marked as the mode transition). The sign of the wall electric field is also inverted after mode transition.

the surfaces, and nearly the entire applied bias is absorbed by bulk plasma. We call this RF plasma *inverted RF plasma* (IRP) as its sheath potential is inverted relative to normal CCP. Note that IRP is fundamentally different from previously observed field reversal in CCP, as the latter is a local and transient effect so the global CCP properties remain unchanged [50,51].

Simulation shows that the electric field in bulk plasma equals $E_{\text{trans}} = \frac{V_{\text{RF}}}{d} \cos(\omega t)$ with d half of the gap distance and V_{RF} half of the total applied voltage amplitude. In Fig. 1(b) total current of normal CCP leads that of inverted RF plasma by nearly $\frac{\pi}{2}$, and the latter coincides with the source voltage in phase. This phenomenon is highly unusual as the RF sheath in CCP contains capacitance $C_{\text{sh}} = a \frac{\epsilon_0 A}{s_{\text{sh}}}$ with A the electrode area, ϵ_0 vacuum permittivity, s_{sh} sheath size, and a a constant depending on model assumptions [30]. In normal CCP the voltage across two capacitive sheaths far exceeds plasma voltage, and current is $\frac{\pi}{2}$ ahead of voltage. The field is much stronger in sheath where strong displacement current J_d fulfills the continuity. Note that in the bulk of CCP the conduction current J_c is dominant as only a weak field penetrates into bulk plasma. Figure 1(c) shows a mode transition from CCP to IRP by increasing Γ_{em} . If the sheath potential in normal CCP is regarded as positive, one can find that the sign of the sheath potential is inverted when Γ_{em} gradually exceeds Γ_{ep} , which is marked as a mode transition in Fig. 1(c). The sign of the wall electric field is inverted as well.

The reason why an IRP behaves as above can be understood considering the flux of plasma electrons. When a wall potential is positive relative to the sheath edge, plasma electron flux is unobstructed. Conduction current and displacement current in normal CCP and IRP are shown in Figs. 2(a) and 2(b) for comparison. The wall potential is negative relative to the sheath edge in CCP, repelling most plasma electrons back, hence the current continuity in the sheath must be fulfilled by a strong displacement current.

This is, however, unnecessary when the wall potential is positive. An intense conduction current travels unimpeded in bulk plasma as well as in the sheath, which is calculated by $J_c = \sigma_p E_{\text{trans}} = \frac{n_0 e^2}{m_e \nu_m} \frac{V_{\text{RF}}}{d} \cos(\omega t) \approx 27.87 \cos(\omega t) \text{ A/m}^2$. Here e is the elementary charge, σ_p is plasma conductivity, E_{trans} is bulk electric field amplitude, and ν_m is collision frequency. Amplitude given by simulation is 23.02 A/m^2 , which is not far from theory.

Flux balance in IRP becomes clear with the above analyses. Figures 2(c) and 2(d) give the distribution functions of two types of RF plasma. Clearly, presheath and sheath accelerate ions and repel plasma electrons in CCP. Conversely, in IRP no Bohm presheath is present, and the mean sheath potential is positive relative to the sheath edge, hence ions are confined but plasma electrons are unimpeded. Meanwhile, Γ_i is diminished in the sheath while Γ_{ep} conserves. Emitted electrons from the boundary are partially reflected back to the surface by the inverse sheath barrier and some penetrate into plasma, leading to an intense electron concentration near boundary. The flux balance is therefore written as $\langle \Gamma_{\text{ep}} + \Gamma_{\text{eref}} - \Gamma_{\text{em}} \rangle_T = 0$ with Γ_{eref} the flux of reflected emitted electrons towards the boundary. Γ_{em} is constant in simulation, possibly representing thermionic emission or photoemission, but it can also be configured as a function of Γ_{ep} due to SEE [52]. The unique particle and power balance in IRP will be analyzed following a theoretical grounding to be established later.

To summarize, when the average plasma electron flux is below the boundary emission ($\langle \Gamma_{\text{ep}} - \Gamma_{\text{em}} \rangle_T < 0$), normal CCP is replaced by IRP because the conventional flux balance ($\langle \Gamma_{\text{ep}} - \Gamma_i - \Gamma_{\text{em}} \rangle_T = 0$) cannot be fulfilled. IRP contains two oscillating electron-rich inverse sheaths where the wall potential relative to the sheath edge is positive. Consequently, ions are confined while plasma electrons are unimpeded. Meanwhile, the lack of sheath capacitance as in CCP is combined with a much stronger conduction current which

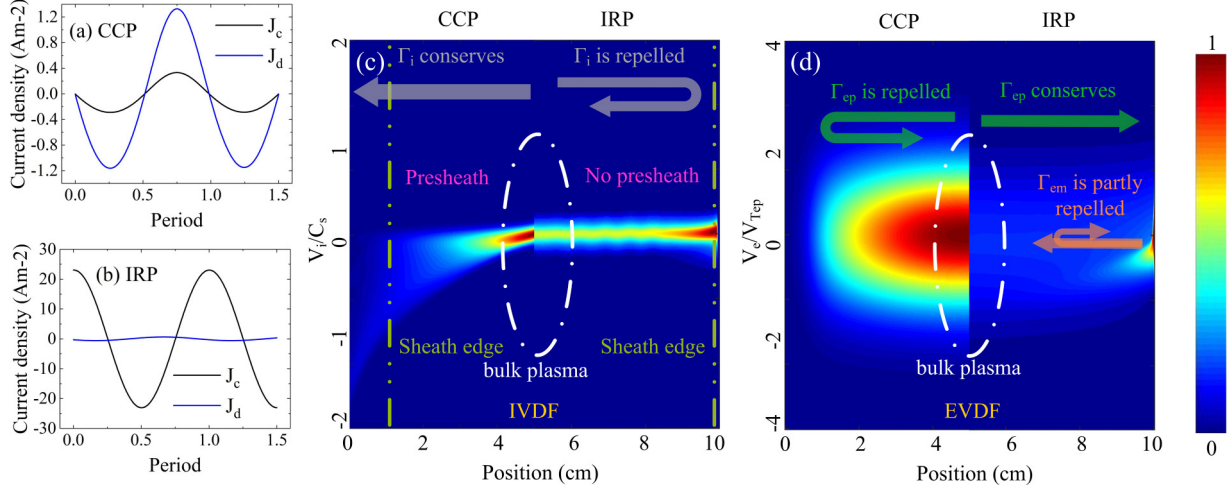


FIG. 2. (a), (b) J_c and J_d in a sheath of CCP and IRP. $J_d \gg J_c$ in a RF sheath of CCP and $J_c \gg J_d$ in inverted RF sheath. (c), (d) Normalized ion and electron velocity distribution functions when $\omega t = 0.5\pi$ for CCP (left panel) and IRP (right panel). Velocity space is normalized to $v_{Tep} = \sqrt{\frac{T_{ep}}{m_e}}$ and $c_s = \sqrt{\frac{T_{ep}}{m_i}}$. (c) Left panel shows that ions are accelerated towards the boundary in CCP and a presheath exists which ensures a minimum velocity when ions enter the sheath. Right panel shows that there is no presheath in IRP and ions are repelled back to plasma by an inverse sheath barrier. The size of a RF sheath in CCP is greater than in IRP. (d) Left panel shows that plasma electrons are repelled in CCP, while right panel shows that in IRP plasma electrons are unimpeded and part of the emitted electrons are repelled back to the surface, forming an intense electron concentration near the surface.

dominates in both bulk plasma and the sheath. Below, a theoretical model will be constructed based on the obtained simulation results.

A step function model is widely used in many CCP theories, which assumes a time-dependent sheath edge out of which the electron density equals zero. In such a model a Child-law-type sheath and Bohm presheath are chosen as a prerequisite [32,33,53,54]. However, existing CCP theories are no longer valid for IRP, and new theoretical ground should be established. Below we will first deduce the inverse sheath potential and then solve the whole IRP. Two key parameters are defined as follows: (1) the mean inverse sheath $\bar{\varphi}_{inv}$ representing the mean potential of the plasma center relative to the wall and (2) the temporal inverse sheath $\varphi_{inv}(\omega t)$ representing the real-time wall potential relative to the sheath edge. The former characterizes ion dynamics, and the latter is for electrons. Both parameters are chosen as positive for simplicity. In Fig. 3 definitions of adopted parameters are shown.

Considering the real-time boundary condition $V_{wall} = \tilde{V} \cos(\omega t)$, the potential difference between plasma center and boundary is expressed as follows according to Fig. 3:

$$-\bar{\varphi}_{inv} + E_{tran}(\omega t)x_s(\omega t) + \varphi_{inv}(\omega t) = V_{RF} \cos(\omega t) \quad (3.1)$$

with x_s the location of sheath edge, so the sheath size is $d - x_s$, and d is the half of gap distance. A simplified expression of temporal inverse sheath barrier is obtained according to the Poisson equation

$$\varphi_{inv}(\omega t) = \frac{\beta en_{sh}}{2\epsilon_0} [d - x_s(\omega t)]^2, \quad (3.2)$$

where β is an adjustable parameter generally equal or greater than one, representing electron density βn_{sh} in an inverted RF sheath. Note that n_{sh} is electron density at the sheath edge. Ions are assumed to be cold and are not considered in an inverse sheath. The assumption used in Eq. (3.2) is analogous

to a previous inverse sheath model for a floating boundary [55].

Using basic plasma kinetic theories, densities of plasma electrons n_{ep} , emitted electrons n_{em} , and reflected emitted electrons n_{eref} in an inverse sheath are derived as follows. Note

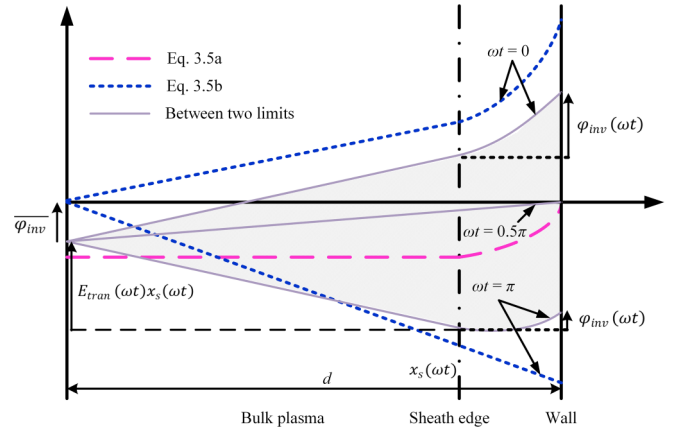


FIG. 3. Schematic of the adopted theoretical model for inverted RF plasma. $\bar{\varphi}_{inv}$ is mean potential of plasma center relative to wall, $\varphi_{inv}(\omega t)$ is real-time wall potential relative to sheath edge, and $E_{tran}(\omega t)x_s(\omega t)$ is sheath edge potential relative to the plasma center. Two limiting cases dictated by Eq. (3.5) are plotted plus normal situations between two limits. Dashed pink curve represents limit of Eq. (3.5a) when no external source is given, which is reduced to a floating inverse sheath. Two dotted blue curves represent the limit of Eq. (3.5b) with an infinite external source, where the mean inverse sheath barrier is eliminated and bulk plasma is directly linked with the boundary without a sheath in a half period. Note that the black dash-dotted line is only an approximation of an inverse sheath edge; actually the position of sheath edge (ωt) is time-dependent, the same as in CCP.

that for convention, we choose $\varphi = 0$ at the sheath edge, the though sheath edge potential is time-dependent relative to the mean potential of the boundary:

$$n_{ep}(\varphi) = n_{ep0} \exp\left(\frac{e\varphi}{T_{ep}}\right) \operatorname{erfc}\left(\sqrt{\frac{e\varphi}{T_{ep}}}\right), \quad (3.3a)$$

$$n_{em}(\varphi) = n_{emw} \exp\left\{\frac{e[\varphi - \varphi_{inv}(\omega t)]}{T_{em}}\right\}, \quad (3.3b)$$

$$n_{eref}(\varphi) = n_{em}(\varphi) \operatorname{erf}\left(\sqrt{\frac{e\varphi}{T_{em}}}\right). \quad (3.3c)$$

Here n_{ep0} is plasma electron density at sheath edge and n_{emw} is emitted electron density at the wall, and deductions of Eq. (3.4) are based on integration of EVDF from the corresponding velocity range, which can be commonly found in many related works on sheath physics [37,55–57]. Taking both the emitted electron and plasma electron flux as half-Maxwellian, we obtain $\Gamma_{ep} = n_{ep0}\sqrt{\frac{2T_{ep}}{\pi m_e}}$, $\Gamma_{em} = n_{emw}\sqrt{\frac{2T_{em}}{\pi m_e}}$. The reflected electron flux is $\Gamma_{eref} = \Gamma_{em}\{1 - \exp[-\frac{e\varphi_{inv}(\omega t)}{T_{em}}]\}$, which is the complement of emitted electrons penetrating the temporal inverse sheath $\Gamma_{em}\exp[-\frac{e\varphi_{inv}(\omega t)}{T_{em}}]$.

In addition, the charge neutrality at the sheath edge must hold, which gives $n_{ep}(\varphi) + n_{em}(\varphi) + n_{eref}(\varphi)|_{\text{sheath edge}} = n_{sh}$. Combining Eqs. (3.1)–(3.3) and charge neutrality, the following relation is obtained:

$$\varphi_{inv}(\omega t) = \frac{(M + \sqrt{M^2 + 4\overline{\varphi_{inv}}})^2}{4} \quad (3.4)$$

with $M = \sqrt{\frac{2\varepsilon_0}{\beta n_{sh}} \frac{V_{RF}}{d}} \cos(\omega t)$. It is then possible to calculate both $\varphi_{inv}(\omega t)$ and $\overline{\varphi_{inv}}$ with the aforementioned flux balance on average $\frac{1}{2\pi} \int_0^{2\pi} (\Gamma_{ep} + \Gamma_{eref} - \Gamma_{em}) d(\omega t) = 0$. The validity of the above deductions can be briefly justified by the dimension and the following two limits:

$$\overline{\varphi_{inv}}|_{V_{RF}=0} = \varphi_{inv}(\omega t)|_{V_{RF}=0} = \frac{T_{em}}{e} \ln\left(\frac{\Gamma_{em}}{\Gamma_{ep}}\right), \quad (3.5a)$$

$$\varphi_{inv}(\omega t)|_{V_{RF} \rightarrow +\infty} = \begin{cases} M^2, & \omega t \in [k\pi, (k+0.5)\pi], \quad k \in \mathbb{Z}^{\geq} \\ 0, & \omega t \notin [k\pi, (k+0.5)\pi], \quad k \in \mathbb{Z}^{\geq} \end{cases} \quad (3.5b)$$

Limits in Eq. (3.5) show that the RF sheath is reduced to a floating inverse sheath when $V_{RF} = 0$. The temporal inverse sheath is rectified in a half period when $V_{RF} \rightarrow +\infty$. Once $\overline{\varphi_{inv}}$ and $\varphi_{inv}(\omega t)$ are determined, the potential in entire the IRP can be calculated by solving Poisson's equation, which requires an order reduction with the numerical integral

$$\left(\frac{d\varphi}{dx}\right)^2 \Big|_0^\varphi = \frac{2n_{ep0}T_{ep}}{\varepsilon_0} \left[\exp\left(\frac{e\varphi}{T_{ep}}\right) - 1 - \mathcal{F}(\varphi, T_{ep}) \right] + \frac{2n_{emw}T_{em}}{\varepsilon_0} \exp\left[-\frac{e\varphi_{inv}(\omega t)}{T_{em}}\right] \left[\exp\left(\frac{e\varphi}{T_{em}}\right) - 1 + \mathcal{F}(\varphi, T_{em}) \right], \quad (3.6)$$

where n_{emw} is given by Γ_{em} , n_{ep0} is solved from charge neutrality, and $\mathcal{F}(\varphi, T) = \exp(\frac{e\varphi}{T}) \operatorname{erf}(\sqrt{\frac{e\varphi}{T}}) - 2\sqrt{\frac{e\varphi}{\pi T}}$.

The integral in Eq. (3.6) is solved from $\frac{d^2\varphi}{dx^2} = \frac{e}{\varepsilon_0} [n_{ep}(\varphi) + n_{em}(\varphi) + n_{eref}(\varphi)]$ multiplied by $\frac{d\varphi}{dx}$ and then integrating over x . Calculated potentials are given in Fig. 4(a), showing good agreement with simulation. The discrepancy of $\overline{\varphi_{inv}}$ is due to assumptions of an ion-free sheath and collisionless sheath, which are not exactly the case in simulation. Figure 4(b) shows $\varphi_{inv}(\omega t)$ with different source voltages. They are normalized by $\overline{\varphi_{inv}}$ to facilitate comparison. For small V_{RF} it is collinear with sinusoidal source, but it gradually approaches the limit of Eq. (3.5b) and becomes rectified at a half period when V_{RF} is large. A complete rectification occurs when $V_{RF} \rightarrow +\infty$, yet a higher ionization rate may shift the realistic condition from the ideal limit. The calculated $\overline{\varphi_{inv}}$ is shown in Fig. 4(c). The mean sheath barrier rises with both Γ_{em} and V_{RF} , making it possible to control the ion confinement by changing the boundary emission and source amplitude. Note that the emission threshold above which IRP is formed increases with V_{RF} .

The abovementioned sheath structure of IRP leads to a unique particle and power balance with respect to normal CCP. For particle balance, ionizations should compensate for ion loss at boundaries. The ion flux conserves in CCP, while only energetic ions crossing $\overline{\varphi_{inv}}$ can hit the wall in IRP, which makes the particle balance different between two types of RF plasma. The general expression of the particle balance is $n_0 K_{iz} n_g d_b = 2\Gamma_{iw}$, with K_{iz} the ionization rate coefficient and Γ_{iw} the ion flux at the wall. Here $d_b = 2\langle x_s \rangle_T$ is the region where ionization occurs, which excludes two sheaths. Note that $\langle x_s \rangle_T$ is the mean RF sheath location relative to the plasma center. In CCP, $\Gamma_{iw} = n_{sh} u_B$ and $n_{sh} = h_l n_0$ with h_l the sheath edge to center density ratio. Note that here the IVDF does not play a role because $T_i \ll e\overline{\varphi_{CCP}}$ with $\overline{\varphi_{CCP}}$ the mean RF sheath potential in CCP (positive). In IRP, it is better to involve IVDF since if not, no ion can pass the mean inverse sheath barrier $\overline{\varphi_{inv}}$ if $T_i < e\overline{\varphi_{inv}}$, which is hardly realistic if the ion temperature becomes remarkable (though not exceeding $e\overline{\varphi_{inv}}$). We consider IVDF in the inverse sheath edge as

$$f_i(v_i) = n_{sh} \begin{cases} \frac{\sqrt{\frac{2m_i}{\pi T_i}}}{1 + \operatorname{erf}\left(\sqrt{\frac{e\overline{\varphi_{inv}}}{T_i}}\right)} \exp\left(-\frac{m_i v_i^2}{2T_i}\right), & v_i \geq v_{i,\min} \\ 0, & v_i < v_{i,\min} \end{cases} \quad (3.7)$$

where $v_{i,\min} = -\sqrt{\frac{2e\overline{\varphi_{inv}}}{m_i}}$. The fact that $f_i = 0$ when $v_i < v_{i,\min}$ is due to an ion loss cone; i.e., energetic ions which cross an inverse sheath barrier cannot return, while those less energetic ions are reflected back. Ion flux towards the wall at the sheath edge is therefore expressed as $\Gamma_{i0} = \frac{n_{sh} \sqrt{\frac{2T_i}{\pi m_i}}}{1 + \operatorname{erf}\left(\sqrt{\frac{e\overline{\varphi_{inv}}}{T_i}}\right)}$. Ac-

cordingly, the ion wall flux in IRP is $\Gamma_{iw} = \Gamma_{i0} \exp(-\frac{e\overline{\varphi_{inv}}}{T_i}) = \frac{n_{sh} \sqrt{\frac{2T_i}{\pi m_i}}}{1 + \operatorname{erf}\left(\sqrt{\frac{e\overline{\varphi_{inv}}}{T_i}}\right)} \exp(-\frac{e\overline{\varphi_{inv}}}{T_i})$. Apparently, since the ion wall flux in IRP is smaller than in CCP, IRP can be sustained with weaker ionization. This also indicates that some ions inevitably flow to the boundary if T_i is remarkable. In deductions of IRP structure it is assumed that no ion presents in inverse sheath, which is based on the assumption that $T_i \ll T_{em}$. It has been shown that a higher ion temperature slightly increases $\overline{\varphi_{inv}}$ [55].

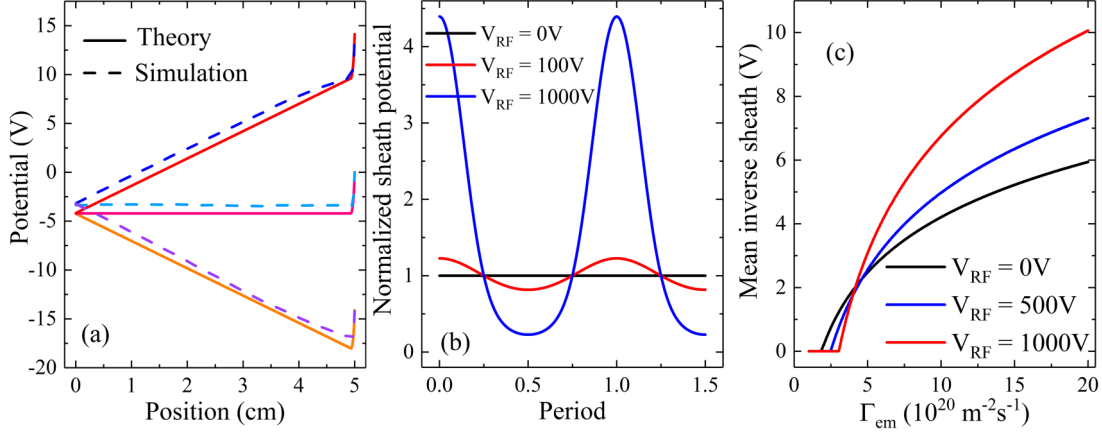


FIG. 4. Results given by theory. (a) The same parameters as in the simulation are used to calculate space potential in IRP at $\omega t = 0, 0.5\pi, \pi$. (b) $\frac{\varphi_{inv}(\omega t)}{\varphi_{inv}}$ at different V_{RF} , unit V. $V_{RF} = 0$ gives a floating inverse sheath [Eq. (3.5a)], sheath potential is sinusoidal for small V_{RF} , for large V_{RF} it is rectified in a half period [Eq. (3.5b)]. (c) φ_{inv} with different Γ_{em} and V_{RF} . The minimum Γ_{em} to invoke IRP increases with V_{RF} , and φ_{inv} increases with Γ_{em} .

The power balance is the balance between power absorption and power loss. The former consists of ohmic heating S_{ohm} and stochastic heating S_{stoc} in CCP, while the latter is due to particle loss at the boundary S_{edge} and interparticle collisions S_{coll} . The electron power balance in CCP is written as [22]

$$S_{coll} + S_{edge} = S_{ohm} + S_{stoc} = S_e \quad (3.8)$$

indicating power lost due to collisions and boundary flux is equal to power gained from ohmic heating and stochastic heating. Note that S terms are power per unit area of electrode. S_e is the power gain or loss of electrons. The LHS is frequently combined as $2\Gamma_{ew}e(\mathcal{E}_c + \mathcal{E}_{e,loss})$ where Γ_{ew} is electron flux at the wall, \mathcal{E}_c is the collisional energy loss per created electron-ion pair, and $\mathcal{E}_{e,loss}$ is the kinetic energy lost per electron lost at the boundary. \mathcal{E}_c is defined by the relation [30]

$$K_{iz}\mathcal{E}_c = K_{iz}\mathcal{E}_{iz} + K_{ex}\mathcal{E}_{ex} + K_{el}\frac{2m_e}{m_i}T_{ep} \quad (3.9)$$

Subscripts iz , ex , and el represent ionization, excitation, and elastic scattering against neutral atoms, respectively, with K and \mathcal{E} the rate coefficients and energy losses of different collision types. In CCP $\mathcal{E}_{e,loss} = 2T_{ep}$ and the corresponding ion energy loss $\mathcal{E}_{i,loss} = 2T_i + \frac{T_{ep}}{2} + e\overline{\varphi_{CCP}}$ where $2T_i$ is frequently neglected as it is much smaller than the others. For IRP, the expression of \mathcal{E}_c is unchanged. For plasma electrons $\mathcal{E}_{ep,loss} = e\overline{\varphi_{inv}} + 2T_{ep}$ and for ions $\mathcal{E}_{i,loss} = 2T_i$. [Rigorously, $\mathcal{E}_{ep,loss}(\omega t)$ is time-dependent because electrons respond to instantaneous potential variation; here we take the average value for simplicity, the same as follows.] This is because the wall potential relative to the sheath edge in IRP is inverted with respect to the RF sheath in CCP, hence incident energies of plasma electrons and ions are inverted as well.

Regarding power absorption, ohmic heating is similar in both types of RF discharge, but IRP contains higher ohmic heating power as its conduction current is intense. It is worthwhile mentioning that the stochastic heating is zero in the inverted RF plasma since its presheath potential is flat. Stochastic heating in normal CCP discharge is due to nonsynchronous motion of the sheath edge and bulk plasma,

which can be verified by current continuity $n_{sh}v_{e,sh,edge} = n_0v_{e,bulk}$, with $v_{e,sh,edge}$, $v_{e,bulk}$ the electron velocity at the sheath edge and bulk plasma, and n_{sh} , n_0 density at sheath edge and bulk plasma, respectively [58]. The drop of plasma density in the Bohm presheath makes $v_{e,sh,edge} \neq v_{e,bulk}$, so a velocity modulation takes place, which cannot happen in an inverted RF plasma where the presheath potential is flat and plasma electron density is uniform. The aforementioned expressions between two types of RF plasma are summarized in Table I for comparison.

A major difference between CCP without boundary emission and IRP is that in IRP there exists a power gain from surface emission and an additional power loss from the flux of reflected surface emission. The power balance of electrons therefore has to be modified as

$$S_{coll} + S_{edge} = S_{ohm} + S_{emis} = S_e \quad (3.10)$$

where S_{emis} is the power of surface emission and is expressed as $S_{emis} = 2\Gamma_{em}e\mathcal{E}_{e,em}$ with $\mathcal{E}_{e,em}$ the kinetic energy gain per emitted electron from the boundary. Note that S_{edge} should contain both plasma electrons and reflected emitted electrons: $S_{edge} = S_{edge,ep} + S_{edge,eref}$. Here $S_{edge,ep} = 2\Gamma_{epw}e\mathcal{E}_{ep,loss}$ and $S_{edge,em} = 2\Gamma_{eref}e\mathcal{E}_{eref,loss}$ with Γ_{epw} plasma electron wall flux and $\mathcal{E}_{eref,loss}$ the kinetic energy lost per reflected electron at the boundary. The expression of $\mathcal{E}_{e,em}$ and $\mathcal{E}_{eref,loss}$ depends on the EVDF of emitted electrons. For half-Maxwellian emitted electrons, $\mathcal{E}_{e,em} = \frac{T_{em}}{2}$ and $\mathcal{E}_{eref,loss} = \langle \frac{1}{\text{erf}[\sqrt{\frac{e\varphi_{inv}(\omega t)}{T_{em}}}]}\{ \frac{T_{em}}{2} - \sqrt{\frac{e\varphi_{inv}(\omega t)T_{em}}{\pi}} \exp[-\frac{e\varphi_{inv}(\omega t)}{T_{em}}] \} \rangle_T$. The expression of $\mathcal{E}_{eref,loss}$ is calculated from the distribution function $f_{eref}(v_e) = n_{eref} \frac{\sqrt{\frac{2m_e}{\pi T_{em}}}}{\text{erf}[\sqrt{\frac{e\varphi_{inv}(\omega t)}{T_{em}}}]}$ $\exp(-\frac{m_e v_e^2}{2T_{em}})$ for $0 < v_e \leq \sqrt{\frac{2e\varphi_{inv}(\omega t)}{m_e}}$ and 0 otherwise (the configuration is the same as in Fig. 3 with the bulk plasma on the left and wall on the right). The missing high-velocity tail in f_{eref} comes from the fact that emitted electrons which cross the inverse sheath cannot return. To complete the discussion of power balance, we note that the total RF power is $S_{RF} = S_e + 2\Gamma_{iw}e\mathcal{E}_{i,loss}$ with the second term

TABLE I. Ion wall flux, kinetic energy lost per plasma electron lost at boundary, kinetic energy lost per ion lost at boundary, ohmic heating power, and stochastic heating power in CCP and IRP. $\overline{\varphi}_{\text{CCP}}$ is mean sheath potential in CCP (positive), $d_b = 2\overline{x}_i$ is the region where ionization occurs (excluding two sheaths).

Type	Γ_{iw}	$\mathcal{E}_{\text{ep,loss}}$	$\mathcal{E}_{i,\text{loss}}$	S_{ohm}	S_{stoc}
CCP	$n_{\text{sh}}u_B$	$2T_{\text{ep}}$	$2T_i + \frac{T_{\text{ep}}}{2} + e\overline{\varphi}_{\text{CCP}}$	$\frac{1}{2}J^2 \frac{d_b}{\sigma_p}$	Nonzero
IRP	$\frac{n_{\text{sh}} \sqrt{\frac{2T_i}{\pi m_i}}}{1 + \text{erf}\left(\sqrt{\frac{e\overline{\varphi}_{\text{inv}}}{T_i}}\right)} \exp\left(-\frac{e\overline{\varphi}_{\text{inv}}}{T_i}\right)$	$e\overline{\varphi}_{\text{inv}} + 2T_{\text{ep}}$	$2T_i$	$\frac{1}{2}J^2 \frac{d_b}{\sigma_p}$	0

on the RHS power loss due to the ion wall flux. This indicates that the total absorbed RF power gets lost through ion wall flux and electron power dissipation. The latter can be further divided into boundary flux loss and collisional power loss. The distinct sheath structure in IRP makes its power balance quite different from that of CCP.

IV. DISCUSSION

An interesting topic still under debate is about the sheath solution for a strongly emissive surface ($\Gamma_{\text{em}} > \Gamma_{\text{ep}}$). Though in this work we report the formation of an inverse sheath in RF plasma, another sheath solution, the SCL sheath, which contains a nonmonotonic space potential, also exists in numerous studies of plasma-surface interaction. Typically, a potential well is formed in front of an electron-emitting surface to reflect part of emission back. The Bohm criterion is still valid in this condition. Actually the sheath is similar to a classical sheath if counted between the potential minimum and bulk plasma. It is seen near the moon and spacecraft surfaces due to secondary electron emission or photoemission [59,60]. Similar results are also observed in positively charged dust grains where conventional orbital-motion-limited (OML) theory is no longer valid [10,61], which can be revised by an OML+ theory [10]. Various potential shapes near macroparticles changing with ion angular moment are also reported by Keider *et al.* [62]. In addition, a SCL sheath due to thermionic emission is reported in emissive probes [37].

In order to control the transition between CCP and IRP, a first method could be monitoring the surface emission, which is considerably difficult if the emission is triggered by secondary electron emission or thermionic emission. The former requires a sudden change of electron energy, while the latter demands a rapid variation of electrode temperature. The fact that there exist two plasma equilibrium states when the boundary emission exceeds plasma electron flux brings a possibility to perform a mode transition easily. It has been shown that under floating or DC condition both a SCL and inverse sheath could exist under certain circumstances [45,48]. A SCL sheath can be maintained only if no cold ion accumulates within the virtual cathode (the potential well), otherwise the VC will be filled due to cold ion trapping and the flux balance will be broken. The cold ion generation is usually caused by charge exchange collision or ionization, hence one may expect a SCL sheath in RF plasma if the ion collision and source terms are closed.

Simulation results show that the above speculations are correct, which implies that the IRP mode can be switched on and off flexibly, as shown in Fig. 5. The simulation in Fig. 5

begins with initial $\Gamma_{\text{em}} = 5 \times 10^{19} \text{ m}^{-2} \text{ s}^{-1}$ ($(\Gamma_{\text{ep}} - \Gamma_{\text{em}})_T > 0$). After discharge becomes stable, Γ_{em} is suddenly augmented to $5 \times 10^{20} \text{ m}^{-2} \text{ s}^{-1}$ ($(\Gamma_{\text{ep}} - \Gamma_{\text{em}})_T < 0$) to trigger the mode transition. In Fig. 5(a) the classical RF sheath gradually collapses after the transition starts. A stable inverted RF plasma is achieved after decades of periods. In the simulation of Fig. 5(b) electron-ion pairs are not generated in the boundary adjacency, and the charge exchange collision is forced to close. It is clear that the SCL RF sheath is formed, and bulk plasma is well isolated from the wall similar to normal CCP. To realize the switch on and off of an inverted RF plasma, one can make use of $\mathbf{E} \times \mathbf{B}$ drift or applying a perpendicular electric field, such that created cold ions can escape from the potential well in other dimensions.

To sustain an IRP in practice, one can capitalize on boundary emission though SEE [63–65], thermionic emission [40,45,46], and photoemission [66–68]. In boundaries of many RF-heated plasma systems, ion flux is damaging, e.g., in a plasma thruster [69], tokamak edge region [70–72], etc. Ion flux induces wall erosion and impurity influx [73,74], which may be eradicated by invoking IRP. The fact that $\overline{\varphi}_{\text{inv}}$ rises with applied voltage makes it possible to confine hot ions with a limited boundary emission, considering that generating very intense Γ_{em} could be difficult in practice. However, caution should be taken as other complexities may appear in practical plasma devices. In a tokamak, for instance, the need to remove helium ash dictates a steady ion flux that should not be minimized independently. Also there exists a strong toroidal magnetic field which dominates over the poloidal field, making an extremely shallow angle at the wall-divertor surface; the emitted electron from the surface would tend to strike back to the surface after completing a gyro-orbit. Therefore, more detailed investigations are needed to make use of the ion flux mitigation effect of IRP in practice.

Another promising prospect of IRP is plasma-based material processing. Ion flux is not easy to control in a collisionless sheath since it conserves. Invoking IRP can monitor ion flux as well as ion incident energy, according to $\Gamma_{iw} = \Gamma_{i0} \exp\left(-\frac{e\overline{\varphi}_{\text{inv}}}{T_i}\right)$ and Table I, with $\overline{\varphi}_{\text{inv}}$ adjustable with respect to Γ_{em} and V_{RF} . The maximum ion flux Γ_{i0} is instantly available by switching IRP off, offering the possibility to control the reaction rate in etching, deposition, synthesis, etc. [30,51,75].

Also, the large RF current in IRP can generate electrostatic waves, which may be further converted into electromagnetic waves. Electrostatic waves can be excited by applying RF voltage on a matched probe immersed in plasma, to be detected and amplified for measurement [76,77]. Strong electrostatic waves generated in IRP can be transformed

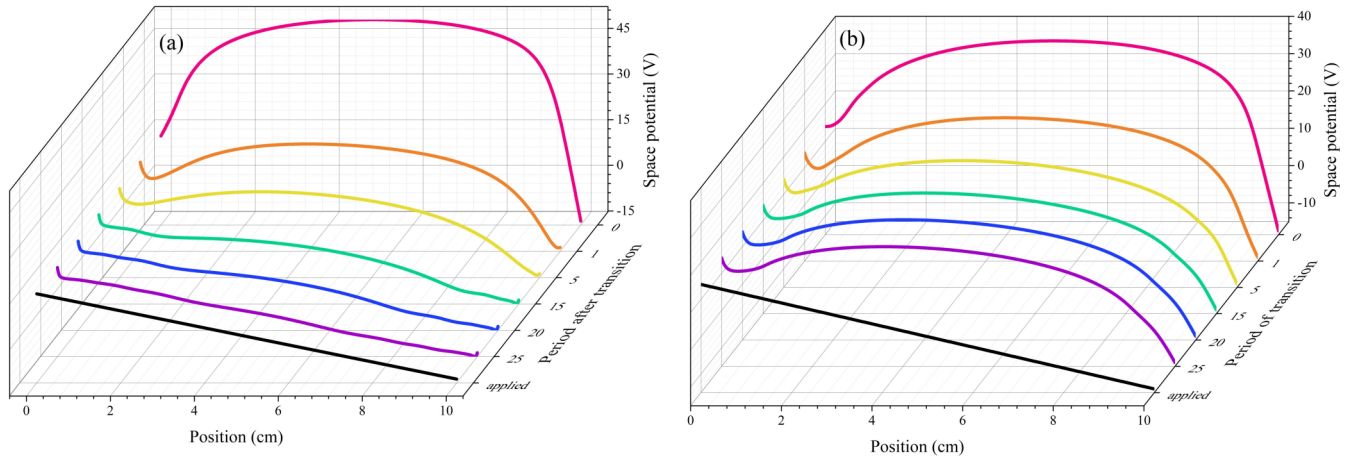


FIG. 5. Time evolution of mode transition. Initially $\Gamma_{em} = 5 \times 10^{19} \text{ m}^{-2} \text{ s}^{-1}$ is given until a stable normal RF sheath is formed. Γ_{em} is suddenly changed to $\Gamma_{em} = 5 \times 10^{20} \text{ m}^{-2} \text{ s}^{-1}$ to initiate the transition. Space potentials within decades of periods during transition are recorded; a straight black curve (front) is applied potential profile in vacuum serving as reference. All data are taken at $\omega t = 0$. (a) Inverted RF plasma mode is switched on, no presheath exists in steady state, and inverse sheath barriers are clearly seen. The bulk plasma is poorly shielded by sheaths and an applied field is unimpeded in plasma. (b) Inverted RF plasma mode is switched off, RF sheath is space-charge limited, ions are unconfined, Bohm criterion is valid, and bulk plasma is well isolated from the boundary with a weak transiting field in plasma bulk.

into electromagnetic radiation through mode conversion in inhomogeneous plasma [78,79], which is expected to be implemented in related experiments.

In the end, instructions will be given to help demonstrate IRP in practice. In some recent works, the existence of an inverse sheath in floating condition has been confirmed experimentally. Wang *et al.* made use of electron-induced secondary electron emission [64]. Secondary electrons are emitted from a stainless steel surface, with emission coefficient controlled by primary electron (PE) energy. A stable inverse sheath is formed with high PE energy (over 100 eV) and intense emitted electron density. Alternatively, Kraus and Raitzes capitalized on thermionic emission [52]. A thoriated tungsten filament is immersed in plasma. When heated, the thermionic current rises until dominating over a plasma electron current, on which a surface potential higher than the plasma potential was observed, consistent with inverse sheath theory. In a typical condition of RF discharge, thermionic emission is encouraged to trigger IRP since secondary electron emission requires a very high electron temperature. A planar 1D configuration with two thermionic emitter seems appropriate.

V. CONCLUSIONS

In conclusion, we show with simulations and on theoretical grounds that boundary emission in RF plasma can produce a strong disturbance, and we establish an inverted RF plasma

different from normal CCP. Applied bias is mainly consumed by bulk plasma instead of a sheath, and the external field is not shielded by the sheath. It naturally confines ions and shows nonclassical sheath coupling, presheath-sheath structure, particle and energy balance, etc. Invoking an inverted RF plasma mitigates ion erosion in a plasma boundary where excessive ion flux is damaging. It also provides inspiration for new reaction control techniques in plasma processing.

ACKNOWLEDGMENTS

G.-Y.S. would like to thank Dr. M.D. Campanell at Lawrence Livermore National Laboratory (LLNL) for his help in modeling and Dr. I. D. Kaganovich and A.V. Khrabrov at the Princeton Plasma Physics Laboratory (PPPL) for fruitful discussions. The authors also thank Prof. Ute Ebert at CWI Amsterdam and Dr. Markus Becker at INP Greifswald for their kind suggestions. This research was conducted under the auspices of the National Natural Science Foundation of China (NSFC) under Grants No. 51827809, No. 51707148, No. U1830129, and No. U1766218.

G.-Y.S. built the simulation mode, conducted data analyses and theoretical deductions, and wrote the manuscript, A.-B.S. helped build the simulation code and theoretical deductions, and G.-J.Z. supervised the work throughout. All authors contributed to the compilation and review of the manuscript.

[1] A. H. Boozer, *Rev. Mod. Phys.* **76**, 1071 (2005).
 [2] A. Fasoli, S. Brunner, W. A. Cooper, J. P. Graves, P. Ricci, O. Sauter, and L. Villard, *Nat. Phys.* **12**, 411 (2016).
 [3] P. K. Shukla and B. Eliasson, *Rev. Mod. Phys.* **81**, 25 (2009).
 [4] M. Nakatsutsumi, Y. Sentoku, A. Korzhimanov, S. N. Chen, S. Buffechoux, A. Kon, B. Atherton, P. Audebert, M. Geissel, and L. Hurd *et al.*, *Nat. Commun.* **9**, 280 (2018).

[5] M. Yamada, R. Kulsrud, and H. Ji, *Rev. Mod. Phys.* **82**, 603 (2010).
 [6] L. Tonks and I. Langmuir, *Phys. Rev.* **34**, 876 (1929).
 [7] T. E. Evans, R. A. Moyer, K. H. Burrell, M. E. Fenstermacher, I. Joseph, A. W. Leonard, T. H. Osborne, G. D. Porter, M. J. Schaffer, and P. B. Snyder *et al.*, *Nat. Phys.* **2**, 419 (2006).

- [8] J. Kates-Harbeck, A. Svyatkovskiy, and W. Tang, *Nature (London)* **568**, 526 (2019).
- [9] G. E. Morfill and A. V. Ivlev, *Rev. Mod. Phys.* **81**, 1353 (2009).
- [10] G. L. Delzanno and X.-Z. Tang, *Phys. Rev. Lett.* **113**, 035002 (2014).
- [11] I. Levchenko, K. Bazaka, Y. Ding, Y. Raitses, S. Mazouffre, T. Henning, P. J. Klar, S. Shinohara, J. Schein, and L. Garrigues *et al.*, *Appl. Phys. Rev.* **5**, 011104 (2018).
- [12] M. D. Campanell, A. V. Khrabrov, and I. D. Kaganovich, *Phys. Rev. Lett.* **108**, 235001 (2012).
- [13] Y.-X. Liu, E. Schüngel, I. Korolov, Z. Donkó, Y.-N. Wang, and J. Schulze, *Phys. Rev. Lett.* **116**, 255002 (2016).
- [14] J. Schulze, A. Derzsi, K. Dittmann, T. Hemke, J. Meichsner, and Z. Donkó, *Phys. Rev. Lett.* **107**, 275001 (2011).
- [15] R. Rajeev, T. Madhu Trivikram, K. P. M. Rishad, V. Narayanan, E. Krishnakumar, and M. Krishnamurthy, *Nat. Phys.* **9**, 185 (2013).
- [16] A. V. Ivlev, J. Bartnick, M. Heinen, C. R. Du, V. Nosenko, and H. Löwen, *Phys. Rev. X* **5**, 011035 (2015).
- [17] B. Bruneau, T. Gans, D. O'Connell, A. Greb, E. V. Johnson, and J.-P. Booth, *Phys. Rev. Lett.* **114**, 125002 (2015).
- [18] M. M. Turner and P. Chabert, *Phys. Rev. Lett.* **96**, 205001 (2006).
- [19] I. D. Kaganovich, *Phys. Rev. Lett.* **89**, 265006 (2002).
- [20] K. Zhao, D.-Q. Wen, Y.-X. Liu, M. A. Lieberman, D. J. Economou, and Y.-N. Wang, *Phys. Rev. Lett.* **122**, 185002 (2019).
- [21] J.-P. Boeuf and B. Chaudhury, *Phys. Rev. Lett.* **111**, 155005 (2013).
- [22] G. R. Misium, A. J. Lichtenberg, and M. A. Lieberman, *J. Vac. Sci. Technol. A* **7**, 1007 (1989).
- [23] T. Lafleur, P. Chabert, and J. P. Booth, *J. Phys. D: Appl. Phys.* **46**, 135201 (2013).
- [24] A. Sun, M. M. Becker, and D. Loffhagen, *Plasma Sources Sci. Technol.* **27**, 054002 (2018).
- [25] G.-H. Liu, X.-Y. Wang, Y.-X. Liu, J.-Y. Sun, and Y.-N. Wang, *Plasma Sources Sci. Technol.* **27**, 064004 (2018).
- [26] K. E. Orlov, D. A. Malik, T. V. Chernoziumskaya, and A. S. Smirnov, *Phys. Rev. Lett.* **92**, 055001 (2004).
- [27] B. Horváth, M. Daksha, I. Korolov, A. Derzsi, and J. Schulze, *Plasma Sources Sci. Technol.* **26**, 124001 (2017).
- [28] Q. Liu, Y. Liu, T. Samir, and Z. Ma, *Phys. Plasmas* **21**, 083511 (2014).
- [29] G.-Y. Sun, H.-W. Li, A.-B. Sun, Y. Li, B.-P. Song, H.-B. Mu, X.-R. Li, and G.-J. Zhang, *Plasma Processes Polym.* **16**, e1900093 (2019).
- [30] M. A. Lieberman and A. J. Lichtenberg, *Principles of Plasma Discharges and Materials Processing, Second Edition* (John Wiley & Sons, Inc., Singapore, 2005).
- [31] T. Lafleur, P. Chabert, and J. P. Booth, *Plasma Sources Sci. Technol.* **23**, 035010 (2014).
- [32] I. D. Kaganovich, O. V. Polomarov, and C. E. Theodosiou, *IEEE Trans. Plasma Sci.* **34**, 696 (2006).
- [33] E. Kawamura, M. A. Lieberman, and A. J. Lichtenberg, *Phys. Plasmas* **21**, 123505 (2014).
- [34] P. Chabert and N. Braithwaite, *Physics of Radio-Frequency Plasmas* (Cambridge University Press, Cambridge, 2011).
- [35] M. M. Turner, *J. Phys. D: Appl. Phys.* **42**, 194008 (2009).
- [36] D. Sydorenko, I. Kaganovich, Y. Raitses, and A. Smolyakov, *Phys. Rev. Lett.* **103**, 145004 (2009).
- [37] J. P. Sheehan, N. Hershkowitz, I. D. Kaganovich, H. Wang, Y. Raitses, E. V. Barnat, B. R. Weatherford, and D. Sydorenko, *Phys. Rev. Lett.* **111**, 075002 (2013).
- [38] A. Autricque, S. A. Khrapak, L. Couëdel, N. Fedorczak, C. Arnas, J. M. Layet, and C. Grisolia, *Phys. Plasmas* **25**, 063701 (2018).
- [39] G. D. Hobbs and J. A. Wesson, *Plasma Phys.* **9**, 85 (1967).
- [40] M. D. Campanell, *Phys. Rev. E* **97**, 043207 (2018).
- [41] M. D. Campanell, A. V. Khrabrov, and I. D. Kaganovich, *Phys. Rev. Lett.* **108**, 255001 (2012).
- [42] J. Juno, A. Hakim, J. TenBarge, E. Shi, and W. Dorland, *J. Comput. Phys.* **353**, 110 (2018).
- [43] D. Coulette and G. Manfredi, *J. Phys.: Conf. Ser.* **561**, 012005 (2014).
- [44] P. Cagas, A. Hakim, J. Juno, and B. Srinivasan, *Phys. Plasmas* **24**, 022118 (2017).
- [45] M. D. Campanell and M. V. Umansky, *Plasma Sources Sci. Technol.* **26**, 124002 (2017).
- [46] M. D. Campanell and G. R. Johnson, *Phys. Rev. Lett.* **122**, 015003 (2019).
- [47] M. D. Campanell and M. V. Umansky, *Phys. Rev. Lett.* **116**, 085003 (2016).
- [48] M. D. Campanell and M. V. Umansky, *Phys. Plasmas* **24**, 057101 (2017).
- [49] X.-Z. Tang and Z. Guo, *Phys. Plasmas* **23**, 120701 (2016).
- [50] J. Schulze, Z. Donkó, B. G. Heil, D. Luggenhölscher, T. Mussenbrock, R. P. Brinkmann, and U. Czarnetzki, *J. Phys. D: Appl. Phys.* **41**, 105214 (2008).
- [51] F. Krüger, S. Wilczek, T. Mussenbrock, and J. Schulze, *Plasma Sources Sci. Technol.* **28**, 075017 (2019).
- [52] B. F. Kraus and Y. Raitses, *Phys. Plasmas* **25**, 030701 (2018).
- [53] M. A. Lieberman, *IEEE Trans. Plasma Sci.* **16**, 638 (1988).
- [54] T. Mussenbrock, R. P. Brinkmann, M. A. Lieberman, A. J. Lichtenberg, and E. Kawamura, *Phys. Rev. Lett.* **101**, 085004 (2008).
- [55] M. D. Campanell, *Phys. Rev. E* **88**, 033103 (2013).
- [56] C. A. Ordonez, *Phys. Fluids B: Plasma Physics* **4**, 778 (1992).
- [57] L. A. Schwager and C. K. Birdsall, *Phys. Fluids B: Plasma Physics* **2**, 1057 (1990).
- [58] E. Kawamura, M. A. Lieberman, and A. J. Lichtenberg, *Phys. Plasmas* **13**, 053506 (2006).
- [59] B. Thiébaud, A. Hilgers, E. Sasot, H. Laakso, P. Escoubet, V. Génot, and J. Forest, *J. Geophys. Res.: Space Phys.* **109** (2004).
- [60] A. Poppe, J. S. Halekas, and M. Horányi, *Geophys. Res. Lett.* **38** (2011).
- [61] G. L. Delzanno, G. Lapenta, and M. Rosenberg, *Phys. Rev. Lett.* **92**, 035002 (2004).
- [62] M. Keidar, I. I. Beilis, R. L. Boxman, and S. Goldsmith, *IEEE Trans. Plasma Sci.* **23**, 902 (1995).
- [63] G.-Y. Sun, Y. Li, S. Zhang, B.-P. Song, H.-B. Mu, B.-H. Guo, A.-B. Sun, and G.-J. Zhang, *Plasma Sources Sci. Technol.* **28**, 055001 (2019).
- [64] X. Wang, J. Pilewski, H. W. Hsu, and M. Horányi, *Geophys. Res. Lett.* **43**, 525 (2016).
- [65] S. Qing and Y. Zhao, *Phys. Plasmas* **25**, 063520 (2018).

- [66] S. Changmai and M. P. Bora, *Phys. Plasmas* **26**, 042113 (2019).
- [67] W. M. Farrell, A. R. Poppe, M. I. Zimmerman, J. S. Halekas, G. T. Delory, and R. M. Killen, *J. Geophys. Res.: Planets* **118**, 1114 (2013).
- [68] M. R. Collier, A. Newheart, A. R. Poppe, H. K. Hills, and W. M. Farrell, *Geophys. Res. Lett.* **44**, 79 (2017).
- [69] E. A. Bering, F. Chang-Diaz, and J. Squire, in *URSI Radio Science Bulletin* (IEEE, Piscataway, 2004), Vol. 2004, pp. 92–106.
- [70] H. Kohno, J. R. Myra, and D. A. D’Ippolito, *Phys. Plasmas* **22**, 072504 (2015).
- [71] B. Angelini, S. V. Annibaldi, M. L. Apicella, G. Apruzzese, E. Barbato, A. Bertocchi, F. Bombarda, C. Bourdelle, A. Bruschi, and P. Buratti *et al.*, *Nucl. Fusion* **45**, S227 (2005).
- [72] A. Cardinali, C. Castaldo, R. Cesario, F. D. Marco, and F. Paoletti, *Nucl. Fusion* **42**, 427 (2002).
- [73] S. T. A. Kumar, D. J. Den Hartog, K. J. Caspary, R. M. Magee, V. V. Mirnov, B. E. Chapman, D. Craig, G. Fiksel, and J. S. Sarff, *Phys. Rev. Lett.* **108**, 125006 (2012).
- [74] X.-Z. Tang and Z. Guo, *Fusion Sci. Technol.* **71**, 110 (2017).
- [75] S. Yatom, R. S. Selinsky, B. E. Koel, and Y. Raitses, *Carbon* **125**, 336 (2017).
- [76] R. N. Franklin, S. M. Hamberger, G. Lampis, G. J. Smith, and D. W. Holder, *Proc. R. Soc. London A* **347**, 1 (1975).
- [77] R. N. Franklin and N. S. J. Braithwaite, *Plasma Sources Sci. Technol.* **18**, 014019 (2008).
- [78] D. E. Hinkel-Lipsker, B. D. Fried, and G. J. Morales, *Phys. Rev. Lett.* **66**, 1862 (1991).
- [79] M. J. Kalaei and Y. Katoh, *Phys. Plasmas* **23**, 072119 (2016).